



Contents lists available at ScienceDirect

# Journal of Industrial and Engineering Chemistry

journal homepage: [www.elsevier.com/locate/jiec](http://www.elsevier.com/locate/jiec)



## Hierarchically mesoporous activated carbon prepared from the dissolution of zinc oxide for high-rate electrical double layer capacitors

Geon-Hyoung An<sup>a</sup>, Do-Young Lee<sup>b</sup>, Hyo-Jin Ahn<sup>a,b,\*</sup>

<sup>a</sup> Program of Materials Science & Engineering, Convergence Institute of Biomedical Engineering and Biomaterials, Seoul National University of Science and Technology, Seoul 139-743, Republic of Korea

<sup>b</sup> Department of Materials Science and Engineering, Seoul National University of Science and Technology, Seoul 139-743, Republic of Korea

### ARTICLE INFO

#### Article history:

Received 27 January 2018

Received in revised form 21 April 2018

Accepted 13 May 2018

Available online xxx

#### Keywords:

Electrical double-layer capacitors

Electrode

Activated carbon

Mesoporous

Rate performance

### ABSTRACT

Due to its highly specific surface area, and excellent chemical stability activated carbon has received a great attention as an electrode material for electrical double-layer capacitors (EDLCs). However, the serious challenge is related to the low mesopore volume fraction of activated carbon, which leads to a low high-rate performance owing to a long path way for ionic diffusion. In the present study, hierarchically mesoporous activated carbon (Meso-AC) was successfully synthesized via the dissolution of zinc oxide (ZnO) nanoparticles during carbonization with the potassium hydroxide activation. In addition, Meso-AC was uniquely derived from protein-based tofu.

© 2018 The Korean Society of Industrial and Engineering Chemistry. Published by Elsevier B.V. All rights reserved.

Due to its highly specific surface area, high electrical conductivity, and outstanding chemical stability, activated carbon has been extensively researched for its potential use in electrochemical capacitors [1–3]. Electrochemical capacitors using activated carbon as the electrode material are attracting scrupulous scientific consideration, as, owing to the unique advantages of high power density, wide range of operating temperature, long cycle stability, and fast charge/discharge rate, these capacitors can liaise the power and energy gap between the traditional capacitors and rechargeable batteries [4–6]. According to the energy storage mechanism with the electrode material, the electrochemical capacitors can be classified into electrical double layer capacitors (EDLCs), pseudocapacitors, and hybrid capacitors [7–10]. Among those, EDLCs hoard charge form electrical double layers between the electrolyte ions and the surfaces of electrode material. In addition, the stored charge is proportional to the specific surface area of electrode materials [11–14].

Most activated carbon as an electrode material was conventionally synthesized from cokes, pitches, and coals, all of which are prone to exhaustion and thus can become less cost-efficient, leading to the exploration of biomass-derived carbon. The seaweed [15], hemp [16], yeast cells [17], dead leaves [18], and fungus [19]

were studied as new raw materials of activated carbon to further increase the specific surface area using a chemical activation. The tofu, which includes protein, water, minerals, omega-3 fatty acids, and vitamins, is one of the unique raw carbon sources and an increasingly popular food [20,21]. The protein is composed of amino acid and carbon atom. Thus, in a previous study, we firstly reported the protein-based tofu for a fabrication of carbon [20,21].

Nevertheless, one of the problems of such fabrication is the low mesopore volume fraction derived from biomass-derived carbon, which leads to a poor high-rate performance due to the long path way for ionic diffusion. This is so because the typical chemical activation using potassium hydroxide (KOH) results in the development of micropores with high surface areas [21]. Therefore, to enhance the high-rate performance of EDLCs, further development of mesoporous structure with a shorter pathway for ionic diffusion in electrode materials is essential.

Hence, in the present study, we performed the fabrication of increased mesopore volume fraction of activated carbon via the dissolution of ZnO nanoparticles during carbonization with the KOH activation. The high specific surface area was developed using the KOH activation. In addition, the dissolution of ZnO foamed the mesoporous structure of activated carbon. As a result, we optimized and demonstrated the between the surface properties, such as specific surface and mesopore volume fraction, and the electrochemical performance for high-performance EDLCs.

\* Corresponding author.

E-mail address: [hjahn@seoultech.ac.kr](mailto:hjahn@seoultech.ac.kr) (H.-J. Ahn).

## Experimental

### Chemicals

Protein used from tofu (Pulmuone Co., Ltd.), zinc oxide (ZnO, <100 nm in size, Sigma–Aldrich), and hydrochloric acid (HCl, Sigma–Aldrich) were purchased. Potassium hydroxide (KOH) was purchased from SAMCHUN.

### Synthesis of hierarchically mesoporous activated carbon (Meso-AC)

The hierarchically mesoporous activated carbon (Meso-AC) was successfully synthesized via the dissolution of ZnO during carbonization. The protein-based tofu was first mixed with ZnO nanoparticles. Afterward the samples dried in an oven at 100 °C to dehydrate. To obtain the mesoporous structure, ZnO nanoparticles were gradually controlled using different amounts of 10, 20, 30 wt.% ZnO, thereafter referred to as Meso-AC 10, Meso-AC 20, and Meso-AC 30, respectively. The prepared samples were carbonized with the KOH activation at 800 °C in N<sub>2</sub> atmosphere and then washed using HCl and DI-water to remove the residue of Zn. For the KOH activation, the amount of KOH was used at the weight ratio of 1:4 (W<sub>Tofu</sub>/W<sub>KOH</sub>). Moreover, we also fabricated activated carbon without ZnO nanoparticles, thereafter referred to as AC.

### Characterization

The structure and morphology were examined by using scanning electron microscopy (SEM) and transmission electron microscopy (TEM, KBSI Gwangju Center). The crystal structure was confirmed by X-ray diffractometry (XRD) by a Cu K $\alpha$  source. The contents were measured using thermogravimetric analysis (TGA) from 200 to 900 °C in air. To investigate the porous structure, Brunauer–Emmett–Teller (BET) and Barrett–Joyner–Halenda (BJH) were executed using N<sub>2</sub> adsorption isotherms.

### Electrochemical analysis

Electrochemical measurements were prepared using the two-electrode system. The electrode pastes were prepared using the Meso-AC as the active material, ketjen black as the conducting

material, and polyvinylidene difluoride as the binder in N-methyl-2-pyrrolidone. The coated electrodes on nickel foam were dried at 100 °C for 2 h. The electrolyte was prepared a 6 M KOH solution. Cyclic voltammetry (CV) was executed using a potentiostat/galvanostat. In the potential range of 0.0–1.0 V, a charging/discharging test was carried out at the current density of 0.2–20.0 A g<sup>-1</sup>. At the current density of 1 A g<sup>-1</sup>, cycling stability of the prepared electrodes was examined up to 2,000 cycles. The specific capacitance was obtained using a discharge curve and the following equation (see Eq. (1)) [10–12,16–19]:

$$C_{sp} = 4I(m dV/dt) \quad (1)$$

where  $I$  (A),  $m$  (g),  $dV$ , and  $dt$  (s) are charging and discharging current, total mass of the active material, voltage drop upon discharging, and total discharging time, respectively.

In addition, the energy density ( $E$ , Wh kg<sup>-1</sup>) and power density ( $P$ , W kg<sup>-1</sup>) were obtained by specific capacitance (see Eqs. (2)–(3)) [10–12,16–19]:

$$E = CV^2/8 \quad (2)$$

$$P = E/dt \quad (3)$$

where  $C$ ,  $V$ , and  $dt$  are specific capacitance, discharging voltage, and total discharge time, respectively.

## Results and discussion

The fabrication process of Meso-AC 20 via the dissolution of ZnO during carbonization with the KOH activation is shown in Fig. 1. The protein-based tofu (see Fig. 1(a)) was first mixed with ZnO nanoparticles to obtain the protein and ZnO nanoparticles composite (see Fig. 1(b)). In the next step, the dried protein and ZnO nanoparticles composite (see Fig. 1(c)) were carbonized with the KOH activation at 800 °C in N<sub>2</sub> atmosphere. ZnO nanoparticles foamed the mesopores via the dissolution of ZnO during carbonization. Thus, Meso-AC 20 (see Fig. 1(d)) was successfully synthesized using the dissolution of ZnO and carbonization with the KOH activation.

Fig. 2 shows low-magnification (Fig. 2(a)–(d)) and high-magnification (Fig. 2(e)–(h)) SEM images of AC, Meso-AC 10,

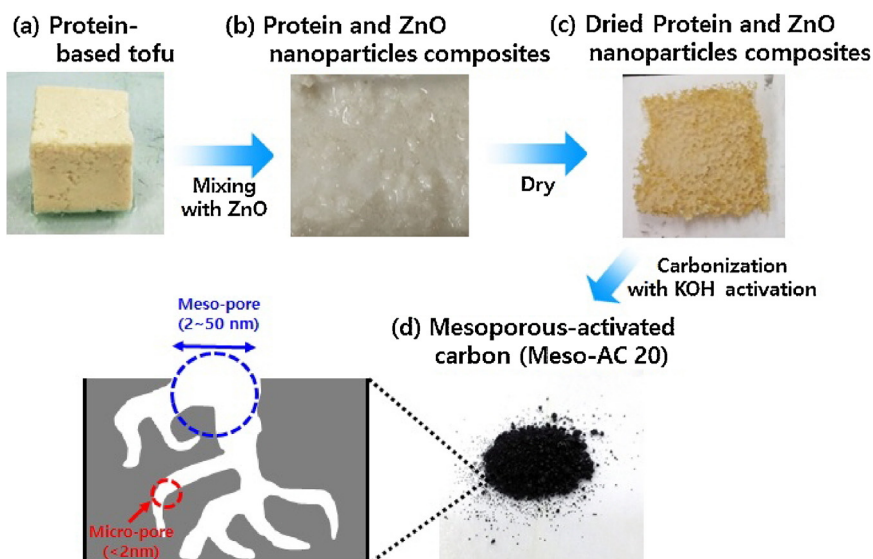


Fig. 1. Schematic illustration of the synthesis procedures for (a) protein-based tofu, (b) protein and ZnO nanoparticles composites, (c) dried Protein and ZnO nanoparticles composites, and (d) mesoporous-activated carbon (Meso-AC 20).

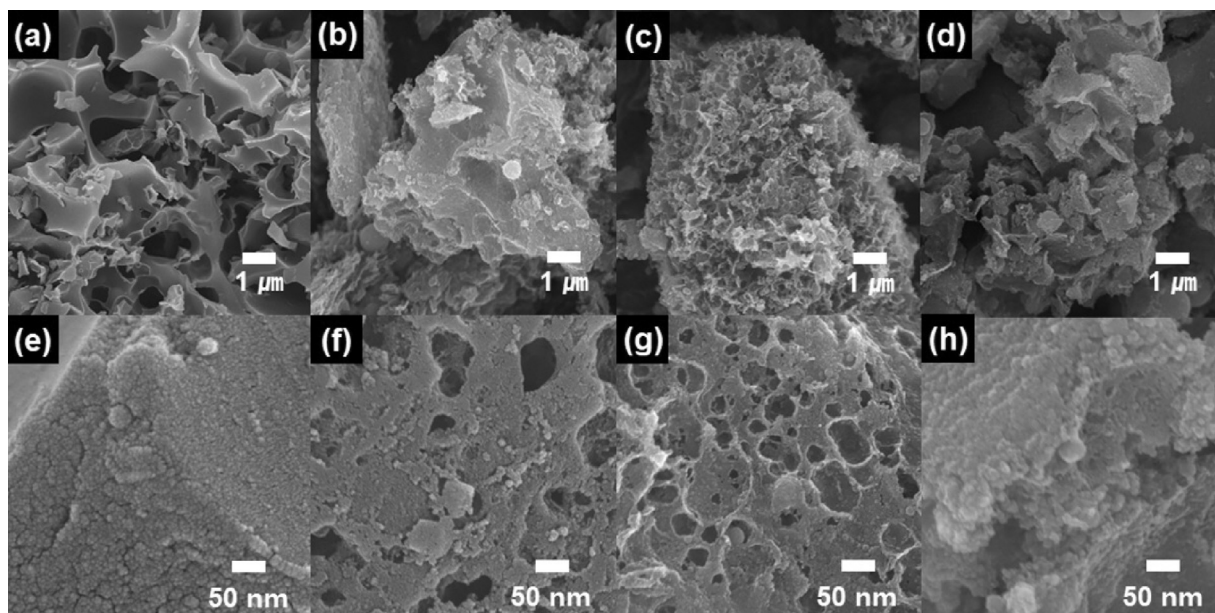


Fig. 2. (a–d) Low-magnification and (e–h) high-magnification SEM images of AC, Meso-AC 10, Meso-AC 20, and Meso-AC 30.

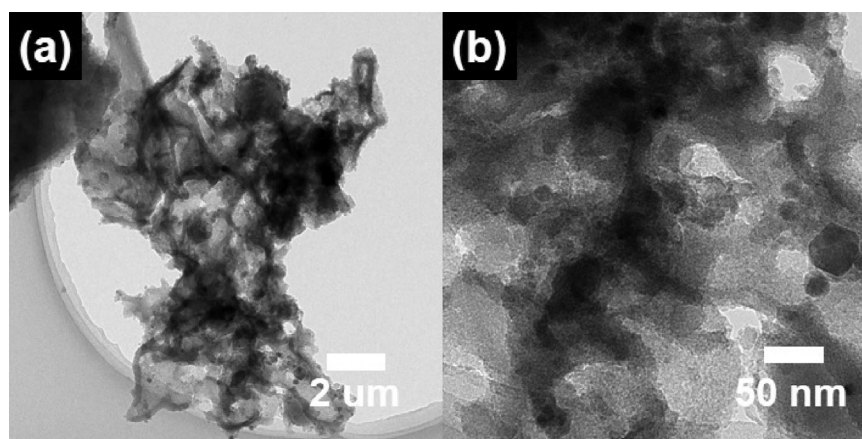


Fig. 3. (a) Low-magnification and (b) high-magnification TEM images of Meso-AC 20.

Meso-AC 20, and Meso-AC 30. All samples had a semi-block morphology with the diameters ranging from 5 to 9  $\mu\text{m}$ . AC (see Fig. 2(a) and (e)) showed smooth surfaces without mesopores. Interestingly, as the relative amount of ZnO nanoparticles increased, the mesoporous structure gradually developed on going from Meso-AC 10 (see Fig. 2(b) and (f)) to Meso-AC 20 (see Fig. 2(c) and (g)) due to the dissolution of ZnO during the carbonization in a  $\text{N}_2$  atmosphere. The embedded ZnO particles in carbon were reduced to Zn and melted over  $419.5^\circ\text{C}$  [22]. Thereafter, the melted Zn were partially evaporated, leading to the formation of a mesoporous structure [22]. The remaining Zn was removed by HCl. Remarkably, Meso-AC 20 displayed the optimized mesoporous structure, resembling a porous honeycomb. However, owing to an excessive amount of ZnO nanoparticles, Meso-AC 30 (see Fig. 2(d) and (h)) presented relatively smooth surfaces, leading to a semi-flake morphology. In other words, the Meso-AC 10 showed the small mesopores owing to a few ZnO nanoparticles with proteins whereas Meso-AC 20 indicated the increased amount of mesopores compared to Meso-AC 10. However, the Meso-AC 30 displayed the relatively smooth surfaces due to an excessive amount of ZnO nanoparticles. Thus, the porous

structure of Meso-AC 20 was optimized using 20 wt.% ZnO nanoparticles with proteins.

To further examine the nanostructural character of Meso-AC 20, the TEM measurement was performed. Meso-AC 20 (see Fig. 3(a) and (b)) displayed a mesoporous structure 51–73 nm in pore size. That is, we fabricated a unique architecture as the electrode material. The developed mesoporous structure is expected to show an improved high-rate performance due to the shorter ion diffusion pathway during cycling.

Fig. 4(a) presents the XRD pattern of AC, Meso-AC 10, Meso-AC 20, and Meso-AC 30 to investigate the crystal structures. The diffraction peak of all samples was located at around  $25^\circ$ , implying the (002) layers of graphite [23,24]. This indicates that the dissolution process of ZnO nanoparticles involved no crystallinity change of carbon. To investigate the content of AC, Meso-AC 10, Meso-AC 20, and Meso-AC 30, the TGA measurement was carried out (see Fig. 4(b)). The weight loss of all samples occurred over  $350^\circ\text{C}$ , implying the decomposition of carbon in air. In addition, all samples showed weight losses of nearly 100%, indicating the existence of pure carbon without impurities. Based on the XRD and TGA results, AC, Meso-AC 10, Meso-AC 20, and Meso-AC 30

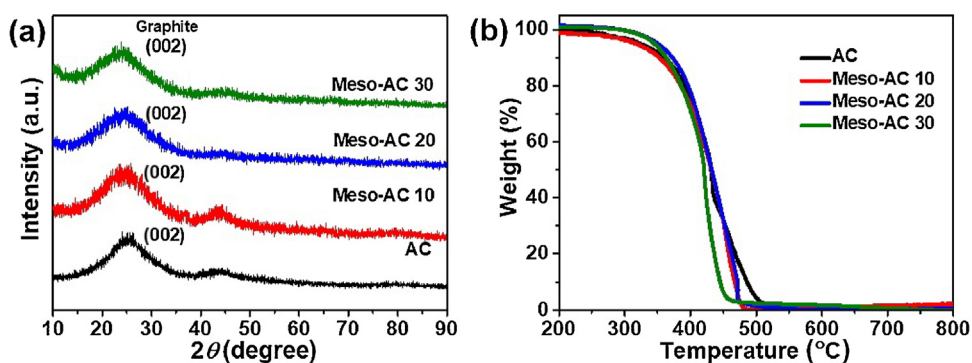


Fig. 4. (a) XRD patterns and (b) TGA curves from 200 to 800 °C at a heating rate of 10 °C min<sup>-1</sup> in air.

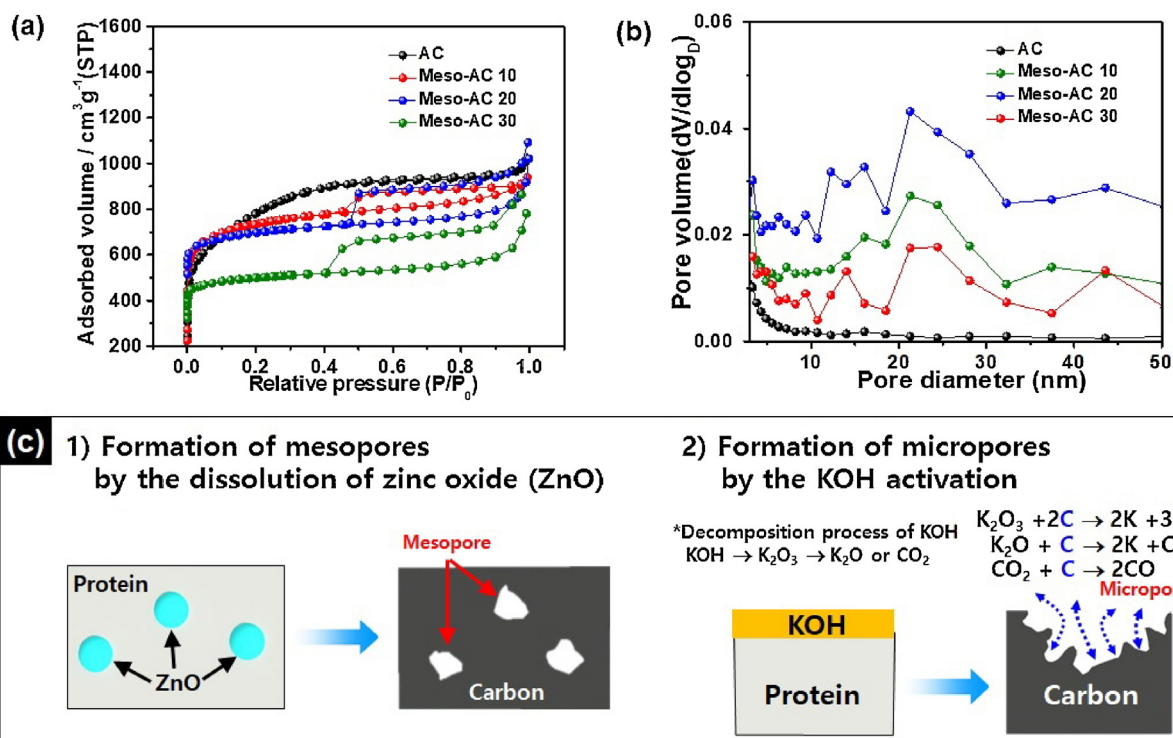


Fig. 5. (a) N<sub>2</sub> adsorption/desorption isotherms. (b) BJH pore size distributions between 0.2 and 50 nm. (c) formation mechanism of Meso-AC 20.

consisting of pure carbon were successfully synthesized using protein-based tofu. These results suggest that protein-based tofu is a novel candidate for a raw material of carbon.

To explore the pore structures, the BET and BJH measurements were performed using N<sub>2</sub> adsorption/desorption isotherms. Fig. 5(a) presents N<sub>2</sub> adsorption/desorption isotherms of AC, Meso-AC 10, Meso-AC 20, and Meso-AC 30. The pore size can divide using micropores (<2 nm) and mesopores (2–50 nm) from the International Union of Pure and Applied Chemistry [11,12]. The isotherm of AC shows Type I features, signifying the existence of micropores (<2 nm). Therefore, the formation of micropores can be ascribed to the pyrolysis between the carbon and KOH during carbonization. The activation procedure for forming micropores can be described by the following reaction:  $\text{KOH} + \text{C} \leftrightarrow \text{K} + \text{H}_2 + \text{K}_2\text{CO}_3$  [21]. On the other hand, the isotherms of Meso-AC 10, Meso-AC 20, and Meso-AC 30 exhibit Type IV features, suggesting the formation of mesopores (2–50 nm) at high pressures ( $P/P_0 > 0.4$ ). As the relative amount of ZnO nanoparticles increased, the mesopore volume fraction steadily increased as well. The mesopore volume fraction of Meso-AC 20 (51%) is 6.3 time higher

than that of AC (8%). Therefore, the mesoporous structure was effectively foamed via the dissolution process of ZnO nanoparticles during carbonization. However, due to the development of the mesoporous structure, the specific surface area of Meso-AC 20 (2,403 m<sup>2</sup> g<sup>-1</sup>) was slightly reduced as compared to AC (2,887 m<sup>2</sup> g<sup>-1</sup>) (Table 1). Fig. 5(b) shows the pore diameter and volume acquired using the BJH measurements. Meso-AC 20 revealed a high pore volume from 2 to 50 nm. The high mesopore volume fraction provides a favorable ionic diffusion at high current densities, leading to an improved electrochemical performance. Based on the SEM, TEM, XRD, BET, and BJH outcomes, the formation mechanism of Meso-AC 20 is illustrated in Fig. 5(c).

To explore the electrochemical feature, in the potential range from 0.0 to 1.0 V, the CV measurements (Fig. 6(a)) were performed at the scan rate of 10 mV s<sup>-1</sup>, in 6 M KOH electrolyte. All electrodes showed a rectangular curve, implying the ideal existence of the electrical double-layer area on the electrode surface. Due to a reduced specific surface area, the CV curve of Meso-AC 20 was slightly smaller than AC. The specific capacitance at the current density range from 0.2 to 20.0 A g<sup>-1</sup> was obtained (see Fig. 6(b)).

**Table 1**

Specific surface area, total pore volume, average pore diameter, and pore volume fraction of AC, Meso-AC 10, Meso-AC 20, and Meso-AC 30.

Samples	$S_{\text{BET}}$ [ $\text{m}^2 \text{g}^{-1}$ ]	Total pore volume ( $p/p_0=0.990$ ) [ $\text{cm}^3 \text{g}^{-1}$ ]	Average pore diameter [nm]	Pore volume fraction	
				$V_{\text{micro}}$ (%)	$V_{\text{meso}}$ (%)
AC	2887	1.5	2.1	92	8
Meso-AC 10	2640	1.8	2.7	71	29
Meso-AC 20	2403	2.4	4.0	49	51
Meso-AC 30	1703	1.5	3.5	58	42

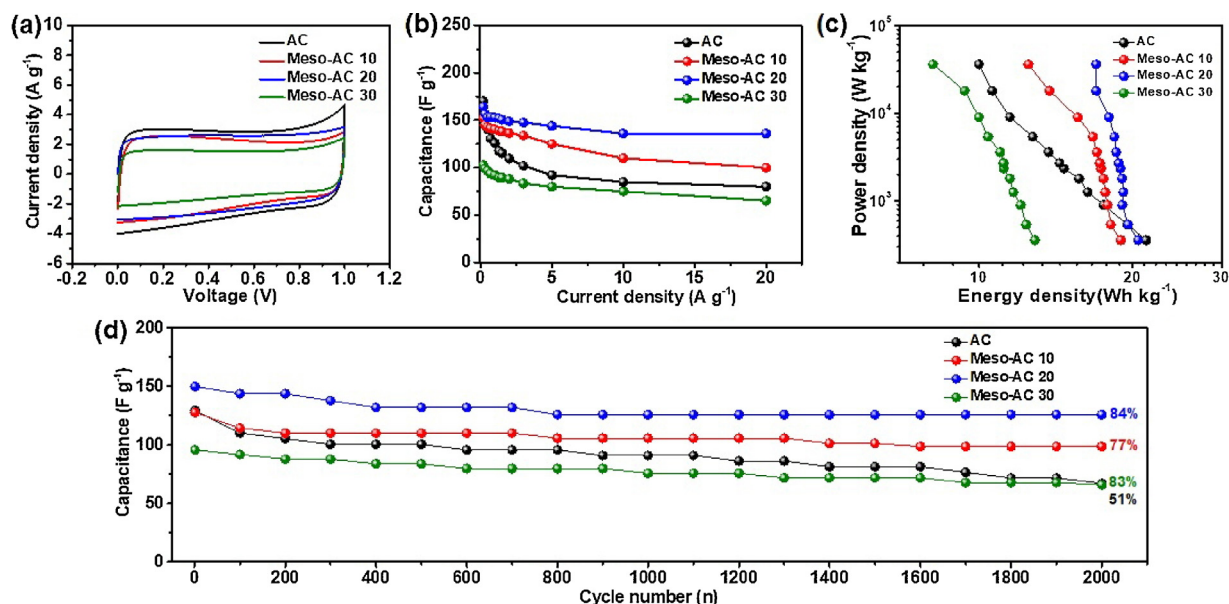


**Fig. 6.** (a) CV curves at scan rate of  $10 \text{ mV s}^{-1}$  in the potential range 0.0 to 1.0 V. (b) Calculated specific capacitance at current densities in the range  $0.2\text{--}20.0 \text{ A g}^{-1}$  in the potential range 0.0 to 1.0 V. (c) Ragone plots related to energy and power densities. (d) Cycling stability at current density of  $1 \text{ A g}^{-1}$  over 2000 cycles.

The specific capacitances of AC, Meso-AC 10, Meso-AC 20, and Meso-AC 30 electrode at the current density of  $0.2 \text{ A g}^{-1}$  were calculated to amount to 170, 152, 164, and  $103 \text{ F g}^{-1}$ , respectively. Due to the high specific surface area, the AC electrode indicated the highest specific capacitance at the current density of  $0.2 \text{ A g}^{-1}$  as compared to other electrodes. However, due to the low mesopore volume fraction, as the current density increased, the specific capacitance of AC electrode rapidly reduced with the low capacitance retention of 46%. On the other hand, due to the decreased specific surface area, the Meso-AC 20 electrode showed a relatively low specific capacitance at the current density of  $0.2 \text{ A g}^{-1}$ . However, at high current densities, the specific capacitances of the Meso-AC 20 electrode were maintained with the high capacitance retention of 82% ( $136 \text{ F g}^{-1}$  at current density of  $20.0 \text{ A g}^{-1}$ ). Therefore, the dissolution process of ZnO for forming the mesoporous structure was optimized by 20 wt% ZnO nanoparticles for high-performance EDLCs. These results demonstrate that the enhanced electrochemical performance with a high capacitance retention may be mainly attributed to the high mesopore volume fraction, which can provide a shorter diffusion pathway and low resistance pathways for the ions because a lot of mesopores are more favorable for ion diffusion at high current densities, based on the efficient utilisation of specific surface areas [11,25]. In the Ragone plot, the energy density and power density were obtained using the specific capacitance values (see Fig. 6(c)). As can be seen in in Fig. 6(c), an energy density reduced with an increase of power density. For the AC electrode with a low mesopore volume fraction, energy density decreased rapidly with an increased power density. Meanwhile, the Meso-AC 20 electrode

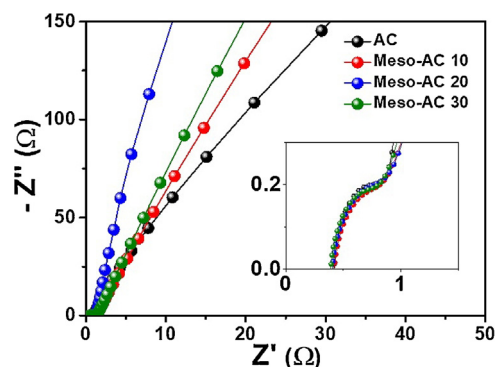


**Fig. 7.** Nyquist plots of the electrodes in the frequency range of  $10^5$  to  $10^{-2}$  Hz at the open-circuit potential.

indicated the high energy density of  $20.5\text{--}17.0 \text{ Wh kg}^{-1}$  in the  $360$  to  $36,000 \text{ W kg}^{-1}$ . To examine the cycling stability, charging and discharging tests at the current density of  $1 \text{ A g}^{-1}$  were performed up to 2000 cycles (see Fig. 6(d)). The Meso-AC 20 electrode displayed an outstanding cycling stability with a high specific capacitance of  $126 \text{ F g}^{-1}$  after 2000 cycles. However, the AC electrode indicated a poor cycling stability with the low specific capacitance of  $67 \text{ F g}^{-1}$  after 2000 cycles, which means the low mesopore volume fraction could affect the inefficient ion transfer during cycling, leading to a poor cycling stability.

Fig. 7 shows the Nyquist plots of electrodes at the open-circuit potential. In the low-frequency range, the straight line is due to the

ionic diffusion ability in the electrode, referred to as the Warburg impedance [25,26]. The Meso-AC 20 electrode is more erect along an imaginary axis than other electrodes, indicating that the enhanced ion diffusion performance is due to the shorter diffusion path way from the increased mesopore volume fraction.

The superb electrochemical performance of Meso-AC 20 electrode was achieved via introducing a novel structure with a highly specific surface area and a high mesopore volume fraction. The first contributing factor here was the introduction of the KOH activation for a highly specific surface area, leading to a high specific capacitance at low current densities. Secondly, the high mesopore volume fraction by the dissolution process of ZnO nanoparticles provided a shorter ionic diffusion pathway, resulting in an outstanding rate performance at high current densities. Until now, ZnO has been applied to optoelectronic devices based on high electron mobility and good chemical stability, but now it can be used as a new technology to form mesopores of carbon [27–30].

## Conclusions

Meso-AC 20 was successfully fabricated via the dissolution of ZnO during carbonization with the KOH activation. Meso-AC 20 with the highly specific surface area of  $2403 \text{ m}^2 \text{ g}^{-1}$  with the high mesopore volume fraction of 51% was optimized by 20 wt% ZnO nanoparticles via a dissolution process during carbonization. The outstanding electrochemical performance of Meso-AC 20 electrode with the high specific capacitance of  $164 \text{ F g}^{-1}$  at the low current density of  $0.2 \text{ A g}^{-1}$ , rate performance ( $136 \text{ F g}^{-1}$  at current density of  $20.0 \text{ A g}^{-1}$ ) with the high capacitance retention of 82% was clearly demonstrated by the following results: (1) the highly specific surface area by the KOH activation could provide the high specific capacitance at a low current density; (2) a high mesopore volume fraction was related to the improved rate performance and excellent cycling stability. Taken together, these results clearly demonstrate that the Meso-AC 20 electrode is a great candidate for subsequent use in high-performance EDLCs.

## Acknowledgments

This research was supported by Basic Science Research Program through the National Research Foundation of Korea (NRF) funded by the Ministry of Science, ICT and Future Planning (NRF-2015R1A1A1A05001252).

## References

- [1] A. Borenstein, O. Hanna, R. Attias, S. Luski, T. Brousseau, D. Aurbach, *J. Mater. Chem. A* 5 (2017) 12653.
- [2] S. Faraji, F.N. Ani, *Renewable Sustainable Energy Rev.* 42 (2015) 823.
- [3] C.Y. Yin, M.K. Aroua, W.M.A.W. Daud, *Sep. Purif. Technol.* 52 (2007) 403.
- [4] P. Simon, Y. Gogotsi, B. Dunn, *Science* 343 (2014) 1210.
- [5] P. Simon, Y. Gogotsi, *Nat. Mater.* 7 (2008) 845.
- [6] G. Wang, L. Zhang, J. Zhang, *Chem. Soc. Rev.* 41 (2012) 797.
- [7] J. Fang, L. Zhana, Y.S. Ok, B. Gao, *J. Ind. Eng. Chem.* 57 (2018) 15.
- [8] S.-K. Chang, Z. Zainal, K.-B. Tan, N.A. Yusoff, W.M.D.W. Yusoff, S.R.S. Prabaharan, *Ceram. Int.* 41 (2015) 1.
- [9] J. Baea, J.Y. Park, O.S. Kwon, C.-S. Lee, *J. Ind. Eng. Chem.* 51 (2017) 1.
- [10] G.-H. An, D.-Y. Lee, H.-J. Ahn, *J. Mater. Chem. A* 5 (2017) 19714.
- [11] G.-H. An, B.-R. Koo, H.-J. Ahn, *Phys. Chem. Chem. Phys.* 18 (2016) 6587.
- [12] G.-H. An, H.-J. Ahn, *Carbon* 65 (2013) 87.
- [13] E.M. Jin, J.G. Lim, S.M. Jeong, *J. Ind. Eng. Chem.* 54 (2017) 421.
- [14] S. Ye, D.C.T. Nguyen, I.-J. Kim, S. Yang, W.-C. Oh, *J. Ind. Eng. Chem.* 54 (2017) 428.
- [15] E. Raymundo-Piñero, F. Leroux, F. Béguin, *Adv. Mater.* 18 (2006) 1877.
- [16] H. Wang, Z. Xu, A. Kohandehghan, Z. Li, K. Cui, X. Tan, T.J. Stephenson, C.K. King'ondo, C.M.B. Holt, B.C. Olsen, J.K. Tak, D. Harfield, A.O. Anyia, D. Mitlin, *ACS Nano* 6 (2013) 5131.
- [17] H. Sun, W. He, C. Zong, L. Lu, *ACS Appl. Mater. Interfaces* 5 (2013) 2261.
- [18] M. Biswal, A. Banerjee, M. Deo, S. Ogale, *Energy Environ. Sci.* 6 (2013) 1249.
- [19] C. Long, X. Chen, L. Jiang, L. Zhi, Z. Fana, *Nano Energy* 12 (2015) 141.
- [20] G.-H. An, D.-Y. Lee, H.-J. Ahn, *J. Alloys Compd.* 722 (2017) 60.
- [21] D.-Y. Lee, G.-H. An, H.-J. Ahn, *J. Alloys Compd.* 52 (2017) 121.
- [22] G.-H. An, D.-Y. Lee, H.-J. Ahn, *ACS Appl. Mater. Interfaces* 9 (2017) 12478.
- [23] G.-H. An, D.-Y. Lee, Y.-J. Lee, H.-J. Ahn, *ACS Appl. Mater. Interfaces* 8 (2016) 30264.
- [24] G.-H. An, H.-J. Ahn, *J. Power Sources* 272 (2014) 828.
- [25] G.-H. An, H.-J. Ahn, W.-K. Hong, *J. Power Sources* 274 (2015) 536.
- [26] G.-H. An, J.I. Sohn, H.-J. Ahn, *J. Mater. Chem. A* 4 (2016) 2049.
- [27] Z. Zang, X. Zeng, J. Du, M. Wang, X. Tang, *Opt. Lett.* 41 (2016) 3463.
- [28] C. Li, Z. Zang, C. Han, Z. Hu, X. Tang, J. Du, Y. Leng, K. Sun, *Nano Energy* 40 (2017) 195.
- [29] C. Li, C. Han, Y. Zhang, Z. Zang, M. Wang, X. Tang, J. Du, *Sol. Energy Mater. Sol. Cells* 172 (2017) 341.
- [30] Z. Zang, *Appl. Phys. Lett.* 112 (2018) 042106.